Physical Aging and Glass Transition of the Rigid Amorphous Fraction in Poly(L-lactic acid)

Xavier Monnier,[1] Dario Cavallo,[2] Maria Cristina Righetti,[3] Maria Laura Di Lorenzo,[4], Sara Marina,[5] Jaime Martin,[5,6] Daniele Cangialosi[1,7]

[1]*Donostia International Physics Center (DIPC), Paseo Manuel de Lardizabal 4, 20018 San Sebastián, Spain*

[2]*Department of Chemistry and Industrial Chemistry, University of Genoa, Via Dodecaneso 31, 16146 Genova, Italy*

[3]*CNR-IPCF, National Research Council - Institute for Chemical and Physical Processes, Via Moruzzi 1, 56124 Pisa, Italy*

[4]*CNR-IPCB, National Research Council - Institute of Polymers, Composites and Biomaterials c/o Comprensorio Olivetti, Via Campi Flegrei, 34, 80078 Pozzuoli (NA), Italy*

[5]*POLYMAT, University of the Basque Country UPV/EHU Av. de Tolosa 72, 20018, San Sebastián, Spain*

[6]*Ikerbasque, Basque Foundation for Science, 48013 Bilbao, Spain*

[7]*Centro de Física de Materiales CFM (CSIC-UPV/EHU) and Materials Physics Center MPC, Paseo Manuel de Lardizabal 5, 20018 San Sebastián, Spain*

Table of Contents (TOC) graphic

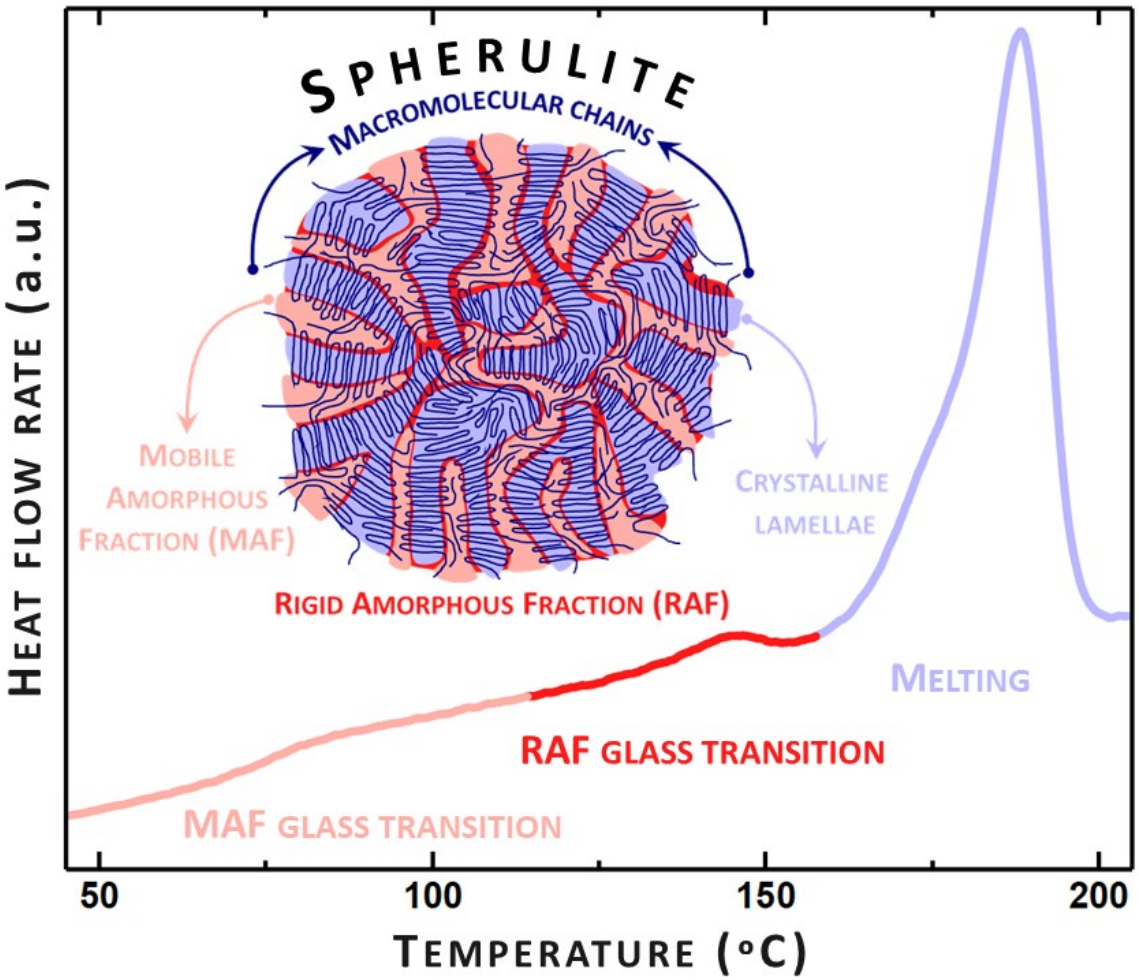

Abstract

The semi-crystalline state of polymers implies the formation of a non-crystalline interphase beside lamellar crystals known as rigid amorphous fraction (RAF). This devitrifies on heating at temperatures much higher than the one typical of the bulk-amorphous fraction. Its glass transition and physical aging in the glassy state has thus far remained elusive. Here, we study the RAF glassy dynamics in poly(L-lactic acid) (PLLA) applying recently developed aging thermal protocols based on fast scanning calorimetry (FSC). Specifically, semi-crystalline samples are aged in different conditions between the glass transition of mobile amorphous fraction and the crystals' melting temperature (Tm). A distinct endothermic peak at temperatures above that of aging develops with time. We provide evidence that in the initial part of aging the origin of this peak is due to the enthalpy recovery of glassy RAF. At longer aging times, the aging peak is at least partly associated to secondary crystallization. Isochronous experiments at different aging temperatures enable to obtain a fair estimate of the RAF glass transition temperature, T_g, whose upper limit is about 135 °C. The proposed method holds the promise of gaining new insights on the elusive glassy dynamics of the RAF of semi-crystalline polymers.

Introduction

The structure of semi-crystalline polymers, as it results from crystallization, comprises a crystalline phase and amorphous fractions of different mobility, as initially highlighted by Wunderlich.[1] The ordered phase creates restraints on the near amorphous areas, with the result that a rigid and disordered nanophase develops at the interphase between crystal lamellae and mobile amorphous areas. This rigid amorphous fraction (RAF) vitrifies/devitrifies at temperatures higher than the glass transition of the mobile amorphous fraction (MAF) (T_g), which is located farther from the crystalline regions.[2,3]

The RAF has been discovered in almost all semi-crystalline polymers[2,3], as well as in a variety of polymeric systems that have alterations in dynamics and glass formation behavior,[4,5] like nanolayered polymers,[6,7] block copolymers,[8] or polymer nanocomposites.[9–13,11] The alterations generally involve a depression in dynamics and an enhancement in T_g when the interface is rigid and well coupled to the polymer.

The RAF largely affects properties of semi-crystalline polymers, like mechanical response, gas permeability and electric conductivity.[14–19] For example, RAF fraction influences the elastic modulus, with a behavior similar to that of the crystal phase, while the gas barrier properties drop because of the higher free volume of the RAF with respect to the crystals. Considering that most large-volume commodity polymers are semi-crystalline, improving knowledge and controlling the RAF has the potential to yield enormous technological and economic benefits.

Large research efforts have been devoted to date to quantify the RAF in a variety of semi-crystalline polymers,[2,3] to study the kinetics of RAF formation and mobilization,[20–26] or the effect of the thermal history,[27–29] as well as the influence of crystal polymorphism on RAF development.[23,30] Due to the various degrees of coupling between the crystallized and the non-crystallized rigid chain portions, RAF vitrifies and devitrifies in a wide temperature range, and progressively decreases with increasing the temperature.[24,25,31] In general, RAF develops simultaneously with the crystal growth

during crystallization at low temperatures, while at higher temperatures it starts to develop during the final stages of the crystallization process, or does not form at all. [24]

Conversely, only few studies have been performed on the time evolution of the RAF structure after crystallization, that is its physical aging[19,32,33] or structural relaxation[34] behavior. Recently it has been proven that both MAF and RAF contribute to structural relaxation in poly(L-lactic acid) (PLLA) upon aging at temperatures below T_g.[25,35–38] RAF does not take part into the cooperative segmental motions close to T_g, because it devitrifies at higher temperatures. Below T_g, RAF partakes in the structural relaxation through small-scale conformational rearrangements, which are barely influenced by the confining crystalline regions.

Due to its glassy nature, RAF can undergo structural relaxation also during aging above T_g, but below the temperature of its complete devitrification. For a few polymers, namely isotactic polystyrene,[39,40] poly(ethylene terephthalate),[41] *cis*-1,4-polybutadiene,[42] poly[(R)-3-hydroxybutyrate],[43] poly(3-(2′-ethyl)hexylthiophene)[41] and poly(3-hexylthiophene) (P3HT),[19,42] a small enthalpy recovery peak subsequent to structural relaxation of the RAF was indeed recognized at the onset of crystal melting. To our knowledge, besides a recent investigation on P3HT,[19] no systematic study on physical aging of the RAF at temperatures higher than T_g of the MAF has ever been conducted, although the occurrence of aging in semi-crystalline polymers at temperatures above T_g was detected by Struik many years ago though the analysis of mechanical properties.[46,47]

In the present study, a complete analysis of the RAF physical aging in a wide temperature range above T_g is reported and discussed for poly(L-lactic acid) (PLLA). This is a bio-based and biodegradable polyester of increasing industrial interest, chosen here for a quantitative analysis of the RAF aging kinetics, because of the wide available knowledge on its three phase structure. The latter includes quantitative data on the kinetics of RAF vitrification in dependence of crystallization temperature[22] and crystal polymorphism,[23] as well as the temperature evolution of the RAF upon non-isothermal crystallization, and the relation with crystal melting.[25]

From the viewpoint of the crystalline phase, PLLA is known to crystallize into two different crystal forms upon quiescent melt or cold crystallization: an ordered α-phase produced at temperatures ≥ 120 °C, and a conformationally disordered (condis) α'-phase that develops at lower temperatures.[48–50] The two polymorphs have only minor differences in the chain packing, linked to conformational disorder and larger unit cell in the α'-modification.[50] The kinetics of crystal nucleation and growth, including the dependence on molar mass and D-lactide comonomer content, has been extensively investigated in the past.[51–53] It was shown that the maximum spherulitic growth rate is encountered at around 125 °C for the α-phase, while nucleation can occur also below T_g, and achieves its fastest kinetics at about 100 °C.

In the present study, we employ fast scanning calorimetry (FSC), complemented with conventional differential scanning calorimetry (DSC) and temperature-modulated differential scanning calorimetry (TMDSC), to provide an in-depth characterization of the physical aging and upper glass transition of the RAF ($T_{g,RAF}$) in PLLA. To this aim, we apply a methodology that relies on the fact that the RAF ages in its glassy state also above the MAF T_g. Hence, the manifestation of physical aging must show the typical calorimetric signature of this phenomenon, that is, the appearance of an endothermic overshoot, implying enthalpy relaxation. This method was firstly introduced to investigate the onset of non-equilibrium effects in polystyrene thin films,[54,55] and later employed to gain insights on the glass transition of P3HT.[19] Here, by changing the aging temperature between T_g and the temperature at which the RAF is formed, i.e. the RAF vitrification/devitrification temperature, we carry out a systematic study on the physical aging behavior of the RAF. In such a way, we also provide an estimate of the upper $T_{g,RAF}$. Incidentally, the proposed in-depth analysis has broader implications for the understanding of so-called “annealing peaks”, commonly observed in semi-crystalline polymers thermally treated below the melting temperature.

Materials and methods

PLLA containing less than 1 % D-isomer co-units, grade name L-175, was kindly provided by Total Corbion (The Netherlands). The melt-flow index is 8 g / 10 min (210 °C/2.16 kg), mass-average and weight-average molar mass are 34 and 106 kDa, respectively, as measured by gel permeation chromatography. PLLA was dried in an oven at 60 °C under vacuum overnight, then compression-molded with a Carver Laboratory Press at a temperature of 190 °C for 2 min, without any applied pressure, to allow complete melting. After this period, a pressure of about 20 bar was applied for 2 min. Successively, the press plates equipped with cooling coils were quickly cooled to room temperature. Film with thickness of about 0.25 mm were obtained.

DSC and TMDSC measurements were performed with a Perkin Elmer Calorimeter DSC 8500 equipped with an IntraCooler III as refrigerating system. The instrument was calibrated in temperature with high purity standards (indium, naphthalene and cyclohexane) according to the procedure for standard DSC. Enthalpy calibration was performed with indium.[56] To gain precise heat capacity data from the heat flow rate measurements, each scan was accompanied by a reference empty pan run. The mass of the aluminum sample pan and empty reference pan matched within 0.02 mg. Dry nitrogen was used as purge gas at a rate of 30 mL min^{-1}.

Before each analysis, PLLA samples were heated from room temperature up to 200 °C at 20 K min^{-1}. An isotherm of 2 min was then performed to erase thermal history. Subsequently, the samples were quenched to 60 °C and left at this temperature for 5 min, to promote homogeneous nucleation.[51] This results in a faster crystallization rate,[53] as well as a higher RAF content.[3] Finally, the samples were heated at 100 K min^{-1} to T_c = 135 °C, and kept at this temperature for 15 min to allow crystallization in the α-form.

At the end of the isothermal crystallization at T_c = 135 °C, PLLA samples were cooled at 50 K min^{-1} to 0 °C, before being either heated by conventional DSC (at rate q_h = 10 K min^{-1}) or by TMDSC (at the average heating rate $q_{h,average}$ = 2 K min^{-1}, with a period of 60 or 120 s, and an amplitude of 0.5 K) until complete melting. According to the mathematical treatment of TMDSC data, the modulated temperature and the heat flow rate curves were approximated to discrete Fourier

series.[57,58] From the ratio between the amplitudes of the first harmonic of the modulated heat flow (A_{HF}) and temperature (A_T), the reversing specific heat capacity ($c_{p,rev}$) was obtained:

$$c_{p,rev}(\omega, T) = \frac{A_{HF}(T)}{A_T(T)} \frac{K(\omega)}{m(\omega)} \quad (1)$$

where ω is the fundamental frequency of temperature modulation ($\omega = 2\pi/p$), m the mass of the sample and $K(\omega)$ the frequency-dependent calibration factor. The average $K(\omega)$ values, determined by calibration with sapphire, were 1.05 ± 0.02 and 1.00 ± 0.02 for p = 60 s and 120 s, respectively. For each measurement, the $K(\omega)$ value was chosen, so that the measured $C_{p,rev}$ values in the glass and melt states matched with the solid ($C_{p,s}$) and liquid ($C_{p,l}$) thermodynamic specific heat capacities, as taken from the literature.[59]

FSC experiments were performed using the Flash DSC 1 of Mettler Toledo with an intracooler, allowing temperature control between −90 and 450 °C, and nitrogen purge. This equipment is based on chip calorimetry and, therefore, allows spanning cooling/heating rates between 0.1 and >1000 K s^{-1}. PLLA samples with mass ~90 ± 10 ng were directly placed on the active area of the chips, and crystallized using the closest possible thermal history used for DSC analyses. As a general rule, all samples were first heated up at 1000 K s^{-1} to 220 ºC, above PLLA melting temperature obtained at such rate (~185 ºC), to remove all previous thermal history. Samples were subsequently exposed to the same protocol used by DSC, that is cooled down to 200 °C (at 1000 K s^{-1}), kept at 200 ºC for 2 min, then cooled down to 60 ºC at 1.67 K s^{-1} (i.e. 100 K min^{-1}) and subjected to a preliminary aging of 5 min to promote homogeneous nucleation. After that, they were immediately heated at 1.67 K s^{-1} to 135 ºC for 15 min to grow crystals from previously formed nuclei. Finally, samples were cooled at 1000 K s^{-1} to a given aging temperature, ranging from 90 and 130 ºC, where isothermal aging was carried out for a wide range of time scales; and subsequently cooled down at 1000 K s^{-1} to -90 ºC and heated up to 220 ºC at the same rate for data recording. For each temperature/time of aging, the FSC profiles of aged PLLA were compared to rejuvenated samples, attained by repeating the thermal history on the same sample, but without the aging step. The entire thermal protocol for FSC experiments is schematized in Fig. 1.

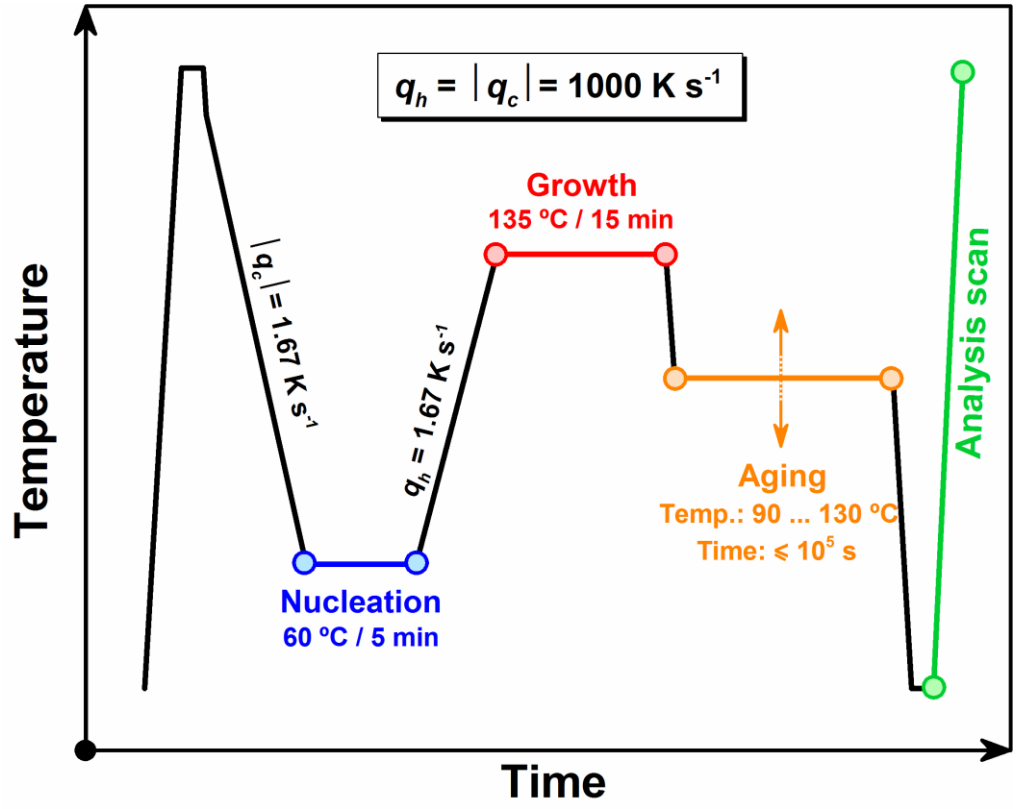

Figure 1. Scheme with the employed thermal protocol for FSC experiments.

Results

In order to quantify the temperature dependence of the RAF, the PLLA samples were analyzed upon heating by DSC and TMDSC, after crystallization at T_c = 135 °C and cooling at 50 K min^{-1} to 0 °C. Figure 2 shows the apparent specific heat capacity ($C_{p,app}$) obtained with DSC, and the reversing specific heat capacities ($C_{p,rev}$) determined by TMDSC at two different modulation periods. As proven by literature data,[35,60] cooling of semi-crystalline PLLA from T_c = 135 °C at 50 K min^{-1} to below T_g does not lead to further crystallization, but only to vitrification of amorphous chain segments.

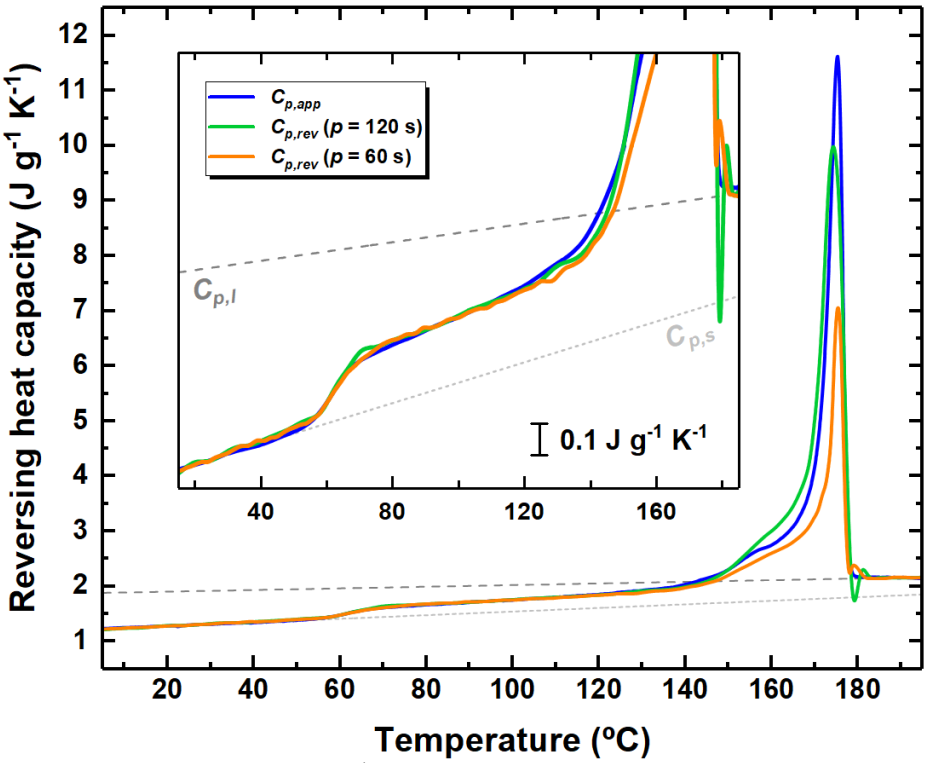

Figure 2. Apparent ($C_{p,app}$, q_h = 10 K min^{-1}) and reversing specific heat capacity ($C_{p,rev}$, $q_{h,average}$ = 2 K min^{-1}, modulation amplitude: 0.5 K, modulation period : 60 and 120 s) of PLLA as a function of temperature after crystallization at T_c = 135 °C. The thin dotted and dashed lines are the thermodynamic solid and liquid specific heat capacities ($C_{p,s}$ and $C_{p,l}$) of PLLA, respectively, as taken from the literature.[59] In the inset, an enlargement of the curves is depicted.

Figure 2 shows that the melting behavior of PLLA after crystallization at T_c = 135 °C is composed by only a peak with a shoulder on the low temperature side, in agreement with previous studies, which demonstrated that when crystallization is performed at T_cs higher than 130 °C, a single melting peak is always observed.[52,53] In the temperature range between T_g, centered at 63 °C, and about 130 °C, the perfect correspondence between the $C_{p,app}$ and the $C_{p,rev}$ indicates that no reversing latent heat is exchanged at temperatures lower than T_c. This proves that, in this temperature range, $C_{p,app}$ and $C_{p,rev}$ correspond to the thermodynamic specific heat capacities of the semi-crystalline PLLA without contribution from latent heat. This allows the quantification of the evolution of the melted fraction (w_{melt}) at temperatures lower than T_c through the following equation:[21]

$$w_{melt}(T) = \frac{C_{p,rev}(T) - C_{p,s}(T)}{C_{p,l}(T) - C_{p,s}(T)} \quad (2)$$

where $C_{p,s}$ and $C_{p,l}$ are the solid and liquid thermodynamic specific heat capacities, respectively, as taken from the literature.[59] Conversely, at higher temperatures, the $C_{p,rev}$ values are different from the corresponding $C_{p,app}$ data, which demonstrates that fusion and reorganization/recrystallization occur upon heating starting from the crystallization temperature, as attested in the literature for other semi-crystalline polymers.[61]

The crystalline fraction (w_C) was determined by using a linear baseline from a temperature slightly below 135 °C (T_i) to the end of the melting (T_f), according to the following equation:

$$w_c(T) = \int_{T_i}^{T_f} \frac{C_p(T) - C_{p,base}(T)}{\Delta h_m^0(T)} dT \quad (3)$$

where $\Delta h_m°(T)$ is the enthalpy of melting of 100 % crystalline α-form.[60] Finally, the vitrified fraction (w_{glassy}) was quantified by difference, i.e., $w_{glassy}(T) = 1 - w_C - w_{liquid}(T)$. At temperatures higher than T_g, w_{liquid} corresponds to the MAF Below T_g, the mobile amorphous fraction vitrifies, w_{liquid} vanishes, and the difference 1-w_C corresponds to the total vitrified amorphous fraction.

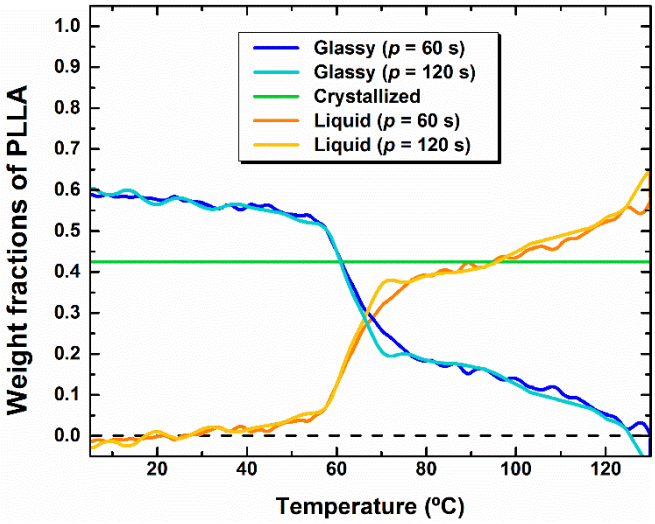

Figure 3. Temperature dependence of vitrified (blue and light blue curves) and mobile (yellow and orange curves) amorphous fractions for PLLA upon heating at 2 K min^{-1} after crystallization at T_c=135 °C and cooling at 50 K min^{-1} to 0 °C. The constant crystalline weight fraction (w_c) value is also indicated. Note that below the $T_{g,}$, the vitrified fraction corresponds to the sum of the MAF and the RAF, whereas above this temperature this is only the RAF.

Figure 3 illustrates the temperature dependence of the MAF and RAF fractions after crystallization at T_c = 135 °C for 30 min. The Figure reveals that at about 70 °C, the RAF amount, that is the portion of material still vitrified, is approximately 0.20. By increasing the temperature, it decreases to become zero at approximately 130 °C. Previous studies demonstrated that the RAF does not develop during crystallization of PLLA at temperatures higher than 130 °C.[37] Thus this temperature was assumed as a limit for the presence of RAF in PLLA. Although the RAF does not form during crystallization at T_c = 135 °C, it can develop upon successive cooling.[35] Due to internal stresses at the amorphous/crystal interface, which are not released during crystal growth, and the progressively reduced chain mobility, amorphous segments can vitrify during cooling at temperatures higher than T_g. This RAF vitrification can occur in a wide temperature range, because the degree of hindrance of the amorphous segments depends on the distance from the crystal.[62]

With the aim of attaining insights on the structural relaxation of PLLA RAF, samples crystallized at 135 ºC by FSC were immediately cooled at 1000 K s^{-1} to aging temperatures ranging from 130 to 90 ºC. An overview of the obtained results is shown in Fig. 4, where the heating scans at 1000 K s^{-1} after aging at different aging temperatures and times are shown. Inspection of Figure 4 evidences the typical calorimetric signature of a semi-crystalline PLLA, that is, the specific heat flow step at ~70 ºC, associated to the MAF T_g, and the melting peak at ~180 ºC. Furthermore, aging between the T_g of the MAF and the melting regions causes the appearance of an excess endotherm with respect to the rejuvenated scan. Such endotherm increases in magnitude with the aging time and progressively shifts to higher temperature with increasing the aging temperature.

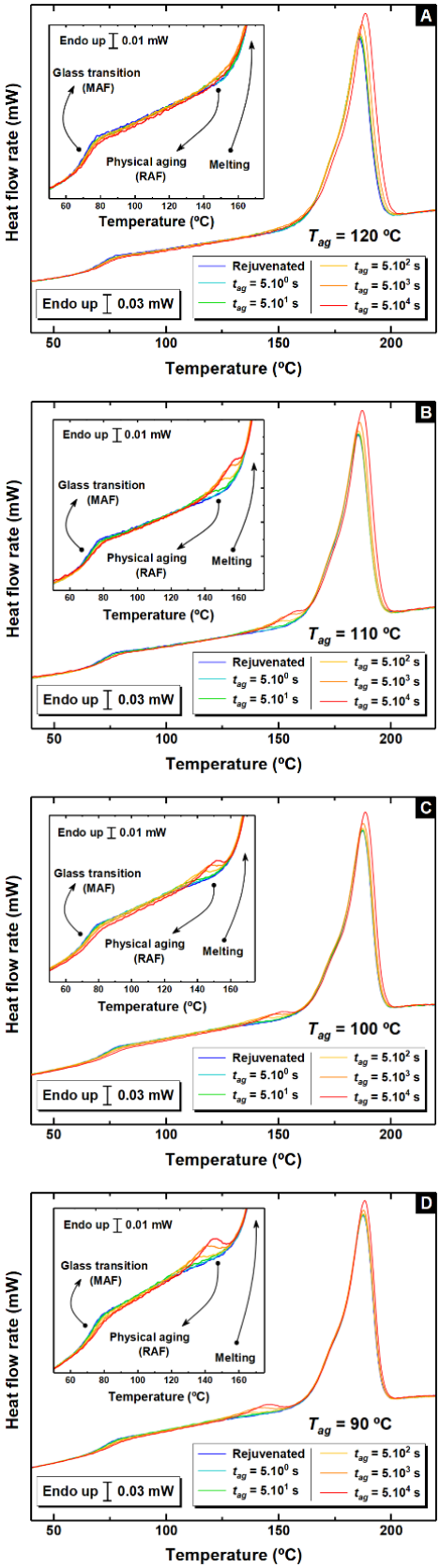

Figure 4. Heating scans after different aging times at the indicated aging temperatures. Insets are magnifications of the T_g region and the temperature range in which the development of the endotherm is observed.

An annealing endothermic peak observed between the T_g of the MAF and primary crystals melting in semi-crystalline polymers has been reported earlier in several studies.[39–42] In order to unveil its origin, we have scrutinized how the evolution of this endothermic peak influences the glass transition of the MAF and the melting of the crystalline phase. The former aspect is shown in Fig. 5A (upper panel), which considers how aging at 100 ºC, as a showcase, affects the step in the specific heat-capacity (ΔC_p) at the MAF glass transition and the corresponding T_g, calculated at ½ ΔC_p. As it can be observed, both quantities essentially remain unaltered until ~2.10^3 s. At longer times, both the specific heat capacity step and the T_g value show time dependent behavior, exhibiting a decrease and an increase, respectively. Similar results are obtained for the modification of the crystallization behavior upon aging at 100 ºC, shown in Fig. 5B (lower panel). This evidences no alteration of the melting behavior, i.e., melting enthalpy and temperature, until ~10^3 s. At longer times, both values increase, indicating improvement of the already existing crystal and/or further growth of crystals. Altogether, these results indicate that while at short aging times the features of the MAF and the crystalline phase remain substantially unaltered, at longer times an increase in the crystalline fraction (secondary crystallization) takes place at expenses of the amount of the MAF and this alters its mobility.

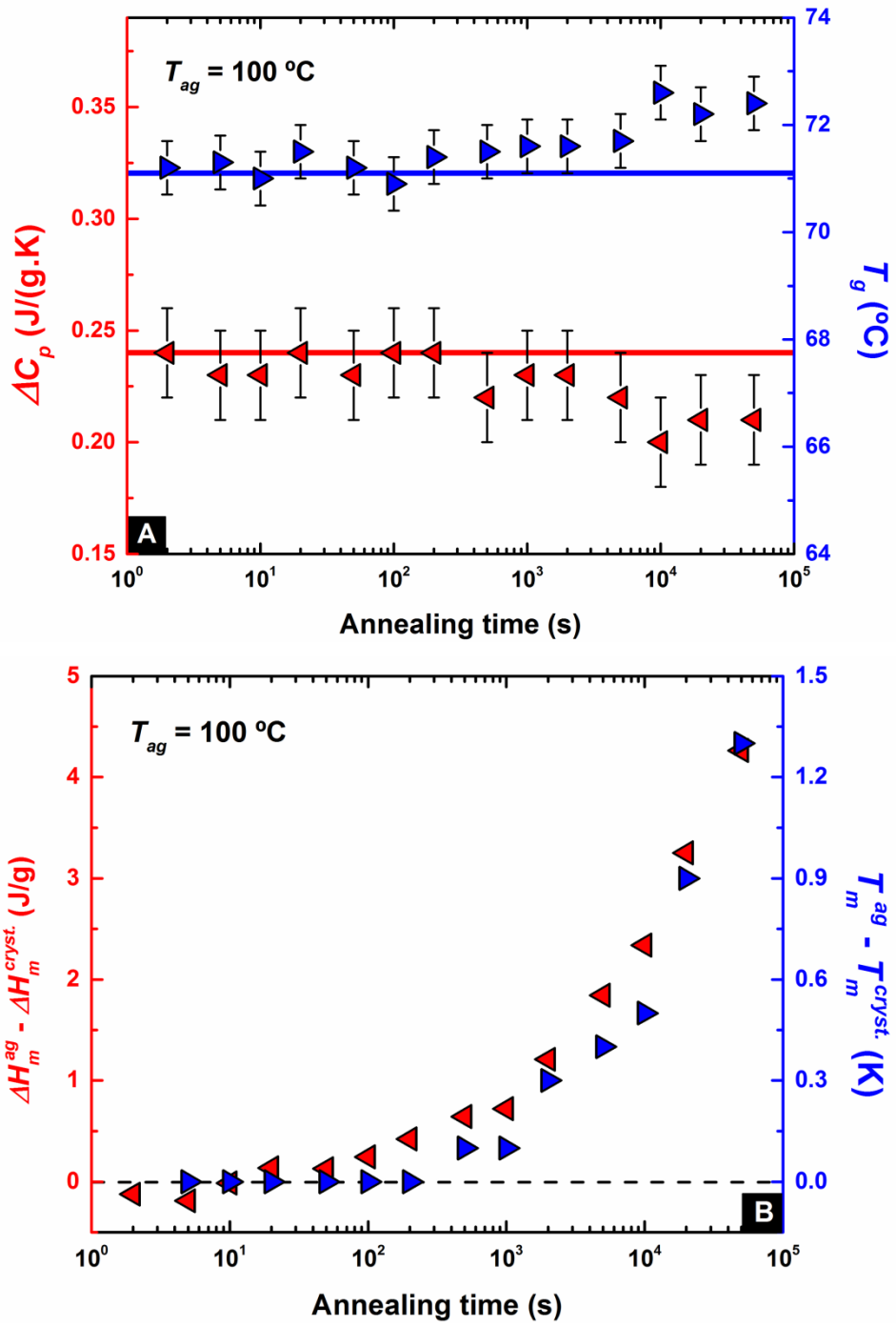

Figure 5. (A) Variation of ΔC_p and T_g with aging times for T_{ag} =100 ºC. (B) Variation of crystal's melting temperature (T_m^{ag}) and melting enthalpy (ΔH_m^{ag}) with aging time, where T_m^{cryst} and ΔH_m^{cryst} are the melting temperature and enthalpy of the rejuvenated sample.

Having identified the connection to secondary crystallization of the endothermic peak at long aging time, we now provide insights on the origin of this peak at shorter time scales. In particular, our aim was to discriminate between two possible scenarios leading to the formation of endothermic

signal, that is, the aging of the RAF or the melting of small crystals formed at large degrees of supercooling. To this aim, we have conveniently adapted a thermal protocol recently proposed by Androsch and Schick.[63] This consists of submitting the samples to multi-step aging experiments at different temperatures in reverse order, i.e., performing in one case aging at relatively high temperature first, followed by a down-jump and aging at a lower temperature, and viceversa in the second case.

The outcome of this analysis is shown in Fig. 6. The upper scans show the specific heat flow rate curves of semi-crystalline PLLA after aging either 90 ºC or at 120 °C for 1000 s and the corresponding reference curves (see green vs. yellow curves). As already shown in Fig. 4D, the aged samples exhibit an aging peak in the range ~120÷150 ºC. A first visual comparison of the quantity of enthalpy produced after these two thermal treatments already suggests that the observed peak is not related to crystallization or ordering phenomena. In fact, given that the crystallization rate (primary or secondary) should increase with aging temperature or at worst being constant in this temperature range,[51] a higher amount of enthalpy should be expected from aging PLLA at 120 °C with respect to 90 °C, when equal times are considered. However, if the peak is not related to the melting/crystals but to physical aging of the RAF, the observed decrease in recovered enthalpy is perfectly understood, in light of the progressively decreasing RAF amount (see Figure 3) and distance from equilibrium with approaching the upper $T_{g,RAF}$.

Further arguments against the crystalline origin of the endothermic effect can be derived by comparing the curves after direct aging at 90 °C with the dual-step aging carried out at 90 ºC and subsequently 120 °C (see green vs. orange curves). In fact, the characteristic peak at around 140°C obtained after 1000 s of aging at 90 °C disappears or is smeared out when a further aging is performed at 120 °C. If this peak were attributed to the melting of small crystallite, it would be hard to understand how these crystals could be erased from the sample by aging it at a temperature (120 °C) below the onset of their melting/disordering. Furthermore, when aging at 120 ºC is followed by aging at 90 ºC, the thermal response is completely different from that induced by simple aging at 120 ºC (see yellow and red curves). If the process occurring during ageing is exclusively

crystallization, the red curve should exhibit an additional melting peak at lower temperature (see article by Furushima), and not a higher peak in the same temperature range (red curve). This event could be ascribed to the reduced relaxation times at 90 °C, which lead to a higher overshoot upon the successive heating.

In contrast, our complex aging experiments are fully compatible with the physical aging scenario. Indeed, it is well known that the appearance of the endothermic overshoot resulting from physical aging depends on the aging temperature.[37,64–66] Specifically, it shifts to lower temperature as the aging temperature is decreased, in line with the outcome of our experiments.

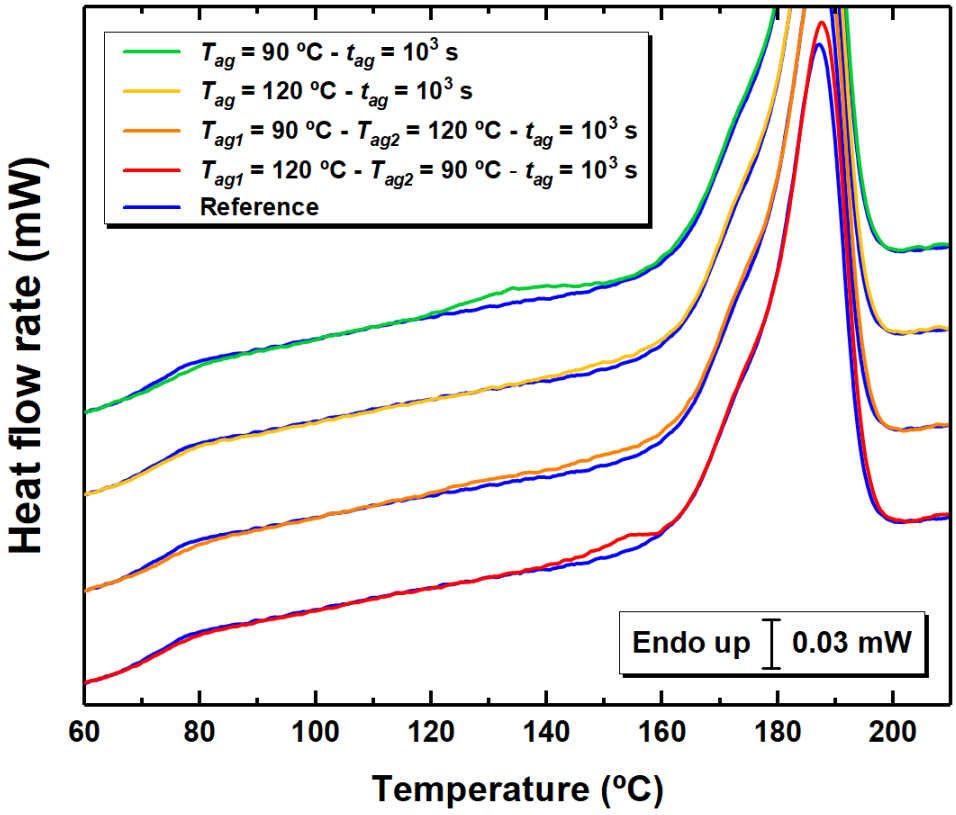

Figure 6. Heat flow rate scans after the indicated thermal protocols. Specifically, when aging is performed only at a single temperature, this is indicated as T_{ag}. A number representing the order of chosen aging temperatures is added as a pedix (i.e., T_{ag1}, T_{ag2}) for two-step aging experiments. In all cases, the aging time is kept fixed among the various steps, and equal to 1000 s.

Having provided arguments that the aging peak observed at relatively short times between the T_g of the MAF and melting temperature is related to RAF physical aging, we now focus on the evolution

of the recovered enthalpy. Details regarding the evaluation of the amount of recovered enthalpy are reported in Fig. 7. Calculation is based on the enthalpy of melting measured for the crystals formed after the nucleation and growth protocol presented in Fig. 1 and the enthalpy of recovery associated to the physical aging of the RAF. From both thermal events, a merged curve is obtained, as highlighted in the inset of Fig. 7, by subtracting a base line (dotted line). By knowing the enthalpy of melting, the enthalpy of recovery is obtained by a simple subtraction from the total area. Firstly, Fig. 8 shows the enthalpy of recovery at four fixed aging times and for various aging temperatures. It is worth noting that for each ageing temperature, only $\Delta H_{recovery}$ data after low ageing times (i.e. before the beginning of the crystallization event) are plotted. As expected, an increase in the aging times implies a general increase of the amount of recovered enthalpy. Here, it is worth noting that for aging times longer than 1000 s, secondary crystallization occurs for T_{ag} < 110 °C. For the largest aging time for which we only observe RAF physical aging, the recovered enthalpy increases linearly with decreasing aging temperature, whereas at lower aging times the typical bell-shaped behavior can be observed. This trend is the results of the antagonist effects of the distance from equilibrium, which increases with decreasing temperature, and of the RAF molecular mobility, exhibiting the opposite behavior. Considering that glass transition is not sharp, i.e., it starts few degrees above $T_{g,RAF}$ midpoint,[38,67] – which is the temperature corresponding to half of the transition – this set of data allows estimating a range of $T_{g,RAF,onset}$, that is, the temperature marking the onset of non-equilibrium effects of the amorphous segments directly linked to the crystals, that is, the most constrained ones. As can be observed in Fig. 8, this is approximately 135 ºC, which agrees well with results by TMDSC showing disappearance of the RAF at about the same temperature (see Figure 3).

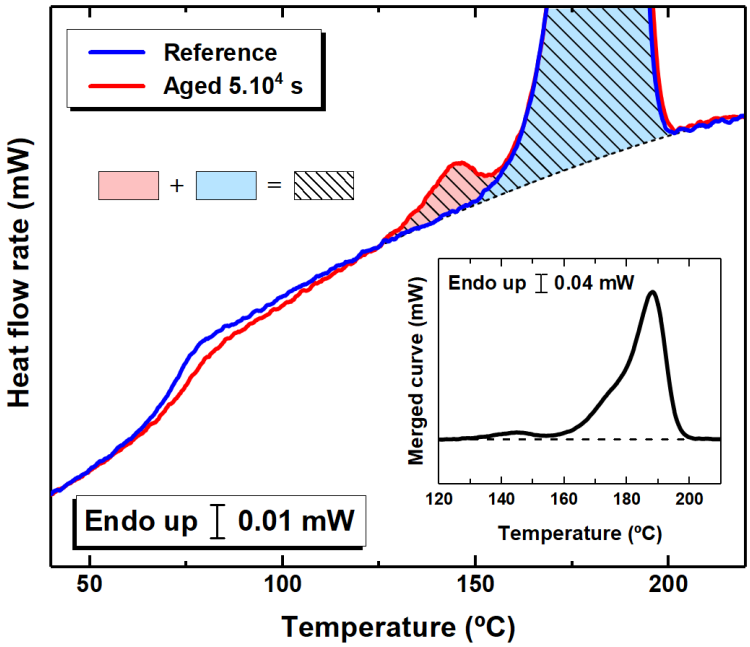

Figure 7. Scheme on the procedure to calculate the recovered enthalpy; here for T_{ag} = 90 °C and t_{ag} = 5.10^4 s, based on the area matching of the reference and the annealed curve. Red area: enthalpy related to the physical aging of the RAF. Blue area: enthalpy of melting related to the crystal formed after nucleation and growth steps specified in Figure 1. The hatched area represents the total enthalpy associated to both thermal events allowing to obtain the merging curve highlighted in the inset.

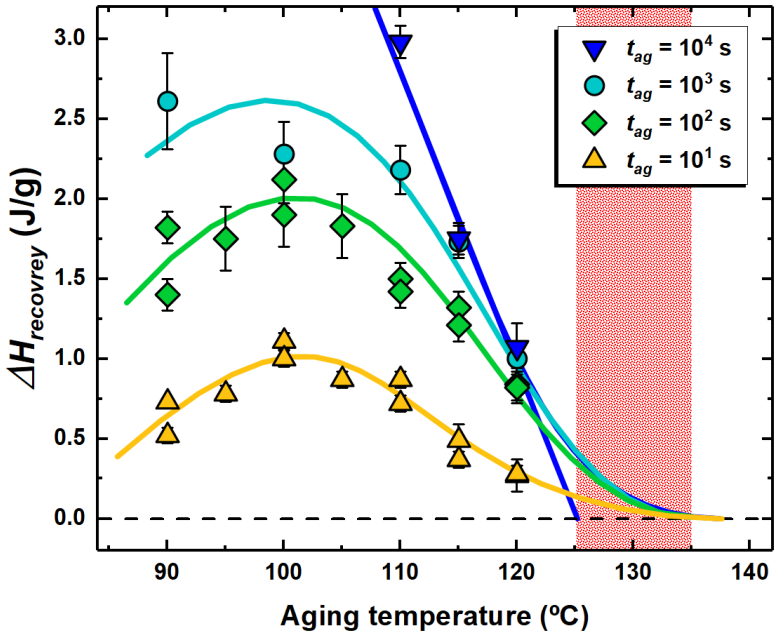

Figure 8. Isochronous recovered enthalpy values as a function of aging temperature for different aging times. The highlighted area illustrates the temperature range of the $T_{g,RAF,onset}$.

Secondly, a complementary view on the equilibrium recovery of glassy RAF is provided in Fig. 9, where the aging time dependence of the recovered enthalpy at different aging temperatures is shown. In this figure, only data at relatively short aging times (blue diamonds) can be attributed to the aging of the RAF, whereas, as previously discussed, data at longer times may be, at least partly, affected by secondary crystallization. All aging data where fitted by the KWW function, which is customarily employed to describe glassy dynamics:[68]

$$\Delta H(t) = \Delta H_{tot} e^{\left(-\frac{t}{\tau}\right)^{\beta}} \quad (4)$$

where τ is the relaxation time of physical aging, β the stretching exponent and ΔH_{tot} the total amount of recoverable enthalpy. As can be observed in Fig. 9, the KWW function provides accurate fit of experimental data. Here it is worth mentioning that the KWW fit only accounts for the non-exponentiality of the relaxation and, therefore, it does not take into consideration the non-linearity of physical aging.[65] Accordingly, the structure dependence of τ, is not considered. The latter generally provides additional stretching to the physical aging behavior. As the structure of RAF submitted to high degree of undercooling is expected to undergo large changes of τ, a decrease of the stretching exponent, β, is anticipated. This trend is actually found when fitting our set of data by the KWW equation as shown in the inset of Fig. 9D. This analysis further corroborates the interpretation of the glassy dynamics nature of the enthalpy evolution observed at relatively short aging times at temperatures between the T_g of the MAF and T_m of the crystal.

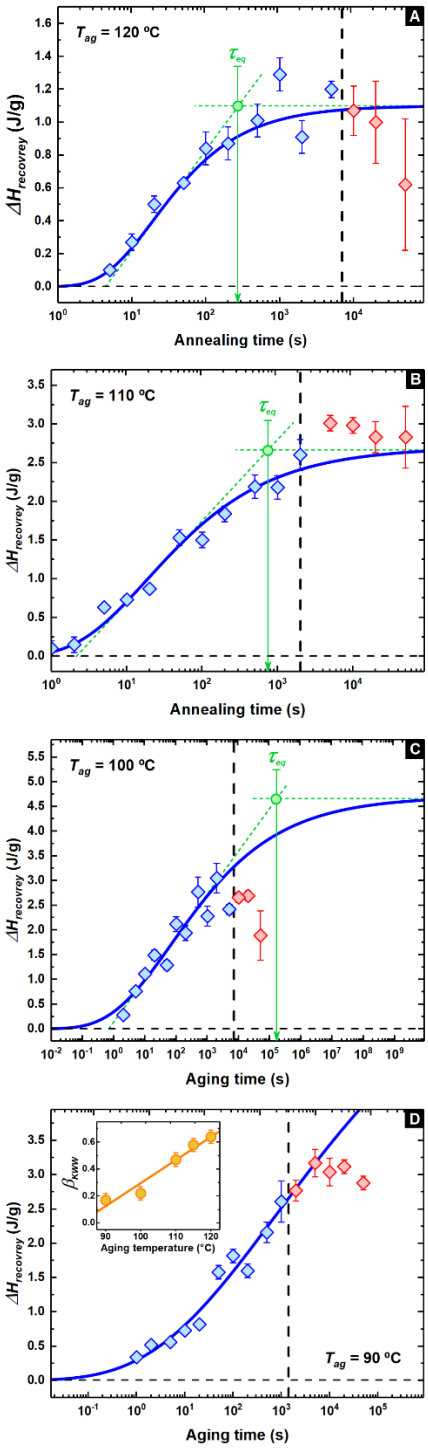

Figure 9. Recovered enthalpy as a function of aging time at different temperatures. Blue diamonds are exclusively related to RAF aging, whereas data represented as red diamonds are affected by secondary crystallization (see text). Inset of Fig. 9D shows the evolution of the stretching exponent β for each investigated aging temperature. The black vertical dashed lines mark the aging time at which secondary crystallization starts.

To provide insights on the time scale involved in the physical aging of the RAF, the model-independent time to reach a plateau of the recovered enthalpy can be extracted from the data shown in Fig. 9. The outcome of this analysis is reported in Fig. 10, where the typical time scales of several processes active in PLLA (primary crystallization, secondary crystallization and physical aging of the RAF) are shown as a function of the inverse temperature. As can be observed, the time scale to reach the plateau of the RAF physical aging, τ_{eq} (green circles), exhibits super-Arrhenius behavior, which is typical of glassy dynamics behavior. Apart from τ_{eq}, different time scales associated to PLLA crystallization can be compared. In particular, the time scales for the onset of secondary crystallization obtained in the present work (see Fig. 4) and those of the half time for primary crystallization taken from refs. 48 and 66 are shown. Interestingly, these time scales, while showing similar trends, exhibit completely different temperature dependence from τ_{eq}. This important result generally indicates that the RAF aging is decoupled from either the primary or secondary crystallization behavior. It is worth noting that, depending on the considered temperature range, the process of secondary crystallization might precede or follow the equilibration of the RAF. This indicates that secondary crystallization can occur concomitantly and in parallel to aging of the RAF. Interestingly, a different situation holds true for the process of primary nucleation, the onset of which has been found at times always larger to MAF structural relaxation in a variety of polymers, including PLLA.[70,71]

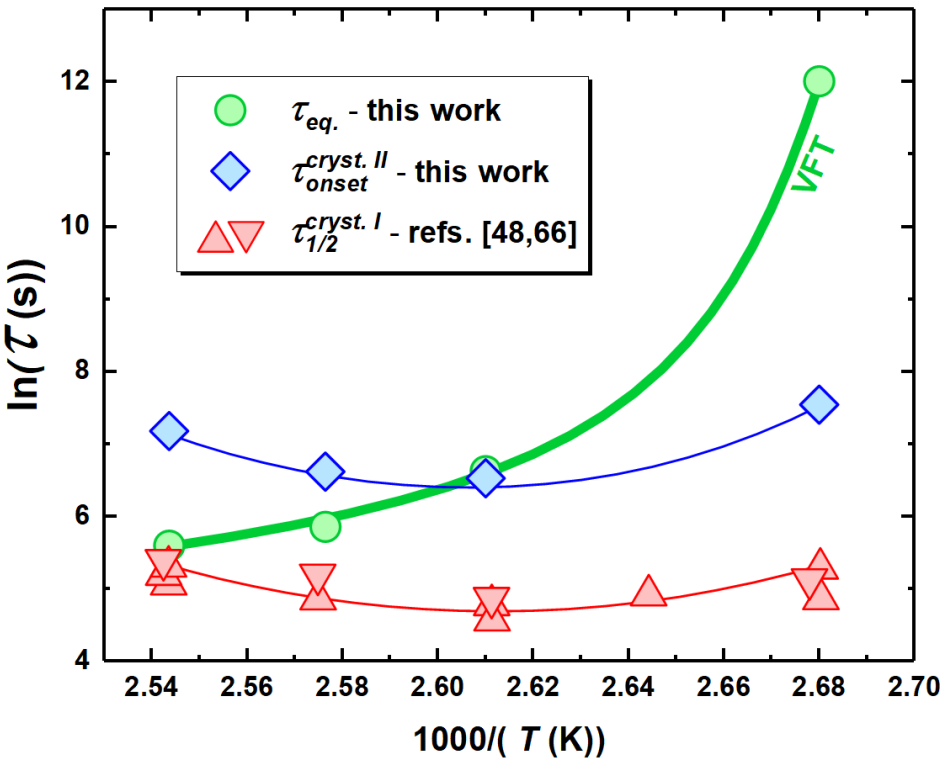

Figure 10. Typical time scales associated to RAF aging and crystallization behavior of PLLA as a function reciprocal temperature.

Discussion and Conclusions

The present study aimed to unveil the origin of the endothermic overshoot exhibited by semi-crystalline polymers between the MAF T_g and T_m when subjected to aging between these two temperatures. The presence of the endothermic overshoot has been subject of intense debate. Two alternative explanations have been proposed: *i)* one is based on the melting of small crystals formed at considerable distance from T_m; *ii)* a second one relies on the physical aging of the RAF, that is, the glassy fraction at the interface between the MAF and the crystalline fraction. Our results on PLLA crystallized in the α form provide strong indications in favor of the latter scenario, under most of the explored conditions. This conclusion is the results of several experimental observations, which are summarized in the following.

Firstly, we show that neither the step at the glass transition nor the temperature and heat of fusion of PLA crystals are modified, once the endothermic overshoot develops. This is the case at least up

a to a certain time scale, depending on the aging temperature. Therefore no modification of primary crystals nor of the amount of MAF takes place during this first stage of aging. A second argument comes from the comparison of the magnitude of the endothermic overshoot after aging for a given time at 90 and 120 ºC, which increases with decreasing temperature, in line with what should be expected for physical aging in glasses, and at odds with the secondary crystallization/melting scenario. Complex aging protocols also provide stringent tests on the nature of the endothermic overshoot. In particular, aging to 120 ºC after a previous aging stage at 90 ºC deeply modified the range and magnitude of the overshoot, in ways not compatible with the crystal melting interpretation. Specifically, there is no reason why crystals formed at 90 ºC and melting above 120 ºC should disappear, once further aging at 120 ºC is carried out. Similarly, aging at 120 ºC followed by aging at 90 ºC produces an aging peak different from that obtained upon aging directly at 90 ºC. While this is an expected result for physical aging, crystallizing at the same final temperature generally provides the same calorimetric signature if crystallization is considered as an explanation. Finally, the decrease of the KWW stretching exponent with decreasing temperature and the super-Arrhenius behavior of the time to reach the plateau in the relaxed enthalpy are two typical signatures of glassy dynamics in non-equilibrium.

Altogether, these results provide convincing evidence that aging between the MAF T_g and T_m induces the development of an endothermic overshoot whose nature is essentially connected to the RAF physical aging. As an important consequence of this conclusion, our approach also permits estimating the upper $T_{g,RAF}$, taken as the onset of non-equilibrium effect. This matches with the value obtained independently by modulated calorimetry. Hence, the approach followed here can be used to provide a complete characterization of the RAF non-equilibrium glassy dynamics in semi-crystalline polymers, where no heat capacity step linked to the RAF glass transition is observed.

Acknowledgements

The authors wish to thank Total Corbion (The Netherlands) for kindly providing PLLA, as well as Dr. Barbara Immirzi of IPCB-CNR for GPC analyses. D. C. acknowledges funding from Spanish Government “Ministerio de Ciencia, Innovacion y Universidades” (PGC2018-094548-B-I00 (MCIU/AEI/FEDER, UE)), and Basque Government (IT-1175-19).

References

(1) Suzuki, H.; Grebowicz, J.; Wunderlich, B. Glass Transition of Poly(oxymethylene). *Br. Polym. J.* **1985**, *17* (1), 1–3. https://doi.org/10.1002/pi.4980170101.

(2) Wunderlich, B. Reversible Crystallization and the Rigid–amorphous Phase in Semicrystalline Macromolecules. *Prog. Polym. Sci.* **2003**, *28* (3), 383–450. https://doi.org/10.1016/S0079-6700(02)00085-0.

(3) Di Lorenzo, M. L.; Righetti, M. C. Crystallization-Induced Formation of Rigid Amorphous Fraction. *Polym. Cryst.* **2018**, *1* (2), e10023. https://doi.org/10.1002/pcr2.10023.

(4) Lee, J.; Mangalara, J. H.; Simmons, D. S. Correspondence between the Rigid Amorphous Fraction and Nanoconfinement Effects on Glass Formation. *J. Polym. Sci. Part B Polym. Phys.* **2017**, *55* (12), 907–918. https://doi.org/10.1002/polb.24324.

(5) Cangialosi, D.; Alegría, A.; Colmenero, J. Effect of Nanostructure on the Thermal Glass Transition and Physical Aging in Polymer Materials. *Prog. Polym. Sci.* **2016**, *54–55*, 128–147. https://doi.org/10.1016/j.progpolymsci.2015.10.005.

(6) Lang, R. J.; Simmons, D. S. Interfacial Dynamic Length Scales in the Glass Transition of a Model Freestanding Polymer Film and Their Connection to Cooperative Motion. *Macromolecules* **2013**, *46* (24), 9818–9825. https://doi.org/10.1021/ma401525q.

(7) Arabeche, K.; Delbreilh, L.; Saiter, J. M.; Michler, G. H.; Adhikari, R.; Baer, E. Fragility and Molecular Mobility in Micro- and Nano-Layered PC/PMMA Films. *Polymer* **2014**, *55* (6), 1546–1551. https://doi.org/10.1016/j.polymer.2014.02.006.

(8) Slimani, M. Z.; Moreno, A. J.; Rossi, G.; Colmenero, J. Dynamic Heterogeneity in Random and Gradient Copolymers: A Computational Investigation. *Macromolecules* **2013**, *46* (12), 5066–5079. https://doi.org/10.1021/ma400577d.

(9) Leng, J.; Szymoniak, P.; Kang, N.-J.; Wang, D.-Y.; Wurm, A.; Schick, C.; Schönhals, A. Influence of Interfaces on the Crystallization Behavior and the Rigid Amorphous Phase of Poly(l-Lactide)-Based

Nanocomposites with Different Layered Doubled Hydroxides as Nanofiller. *Polymer* **2019**, *184*, 121929. https://doi.org/10.1016/j.polymer.2019.121929.

(10) Szymoniak, P.; R. Pauw, B.; Qu, X.; Schoenhals, A. COMPETITION OF NANOPARTICLE-INDUCED MOBILIZATION AND IMMOBILIZATION EFFECTS ON SEGMENTAL DYNAMICS OF AN EPOXY-BASED NANOCOMPOSITE. *Soft Matter* **2020**. https://doi.org/10.1039/D0SM00744G.

(11) Cangialosi, D.; Boucher, V. M.; Alegría, A.; Colmenero, J. Physical Aging in Polymers and Polymer Nanocomposites: Recent Results and Open Questions. *Soft Matter* **2013**, *9* (36), 8619–8630. https://doi.org/10.1039/C3SM51077H.

(12) Wurm, A.; Ismail, M.; Kretzschmar, B.; Pospiech, D.; Schick, C. Retarded Crystallization in Polyamide/Layered Silicates Nanocomposites Caused by an Immobilized Interphase. *Macromolecules* **2010**, *43* (3), 1480–1487. https://doi.org/10.1021/ma902175r.

(13) Sargsyan, A.; Tonoyan, A.; Davtyan, S.; Schick, C. The Amount of Immobilized Polymer in PMMA SiO2 Nanocomposites Determined from Calorimetric Data. *Eur. Polym. J.* **2007**, *43* (8), 3113–3127. https://doi.org/10.1016/j.eurpolymj.2007.05.011.

(14) Lin, J.; Shenogin, S.; Nazarenko, S. Oxygen Solubility and Specific Volume of Rigid Amorphous Fraction in Semicrystalline Poly(ethylene Terephthalate). *Polymer* **2002**, *43* (17), 4733–4743. https://doi.org/10.1016/S0032-3861(02)00278-1.

(15) Di Lorenzo, M. L.; Righetti, M. C. The Three-Phase Structure of Isotactic poly(1-Butene). *Polymer* **2008**, *49* (5), 1323–1331. https://doi.org/10.1016/j.polymer.2008.01.026.

(16) Lin, K. Y.; Xanthos, M.; Sirkar, K. K. Novel Polypropylene Microporous Membranes via Spherulitic Deformation – Processing Perspectives. *Polymer* **2009**, *50* (19), 4671–4682. https://doi.org/10.1016/j.polymer.2009.07.014.

(17) Drieskens, M.; Peeters, R.; Mullens, J.; Franco, D.; Lemstra, P. J.; Hristova-Bogaerds, D. G. Structure versus Properties Relationship of Poly(lactic Acid). I. Effect of Crystallinity on Barrier Properties. *J. Polym. Sci. Part B Polym. Phys.* **2009**, *47* (22), 2247–2258. https://doi.org/10.1002/polb.21822.

(18) Guinault, A.; Sollogoub, C.; Ducruet, V.; Domenek, S. Impact of Crystallinity of Poly(lactide) on Helium and Oxygen Barrier Properties. *Eur. Polym. J.* **2012**, *48* (4), 779–788. https://doi.org/10.1016/j.eurpolymj.2012.01.014.

(19) Martín, J.; Stingelin, N.; Cangialosi, D. Direct Calorimetric Observation of the Rigid Amorphous Fraction in a Semiconducting Polymer. *J. Phys. Chem. Lett.* **2018**, *9* (5), 990–995. https://doi.org/10.1021/acs.jpclett.7b03110.

(20) Schick, C.; Wurm, A.; Mohamed, A. Vitrification and Devitrification of the Rigid Amorphous Fraction of Semicrystalline Polymers Revealed from Frequency-Dependent Heat Capacity. *Colloid Polym. Sci.* **2001**, *279* (8), 800–806. https://doi.org/10.1007/s003960100507.

(21) Schick, C.; Wurm, A.; Mohammed, A. Formation and Disappearance of the Rigid Amorphous Fraction in Semicrystalline Polymers Revealed from Frequency Dependent Heat Capacity. *Thermochim. Acta* **2003**, *396* (1–2), 119–132. https://doi.org/10.1016/S0040-6031(02)00526-9.

(22) Righetti, M. C.; Tombari, E. Crystalline, Mobile Amorphous and Rigid Amorphous Fractions in poly(L-Lactic Acid) by TMDSC. *Thermochim. Acta* **2011**, *522* (1–2), 118–127. https://doi.org/10.1016/j.tca.2010.12.024.

(23) Di Lorenzo, M. L.; Cocca, M.; Malinconico, M. Crystal Polymorphism of Poly(l-Lactic Acid) and Its Influence on Thermal Properties. *Thermochim. Acta* **2011**, *522* (1–2), 110–117. https://doi.org/10.1016/j.tca.2010.12.027.

(24) Righetti, M. C.; Laus, M.; Di Lorenzo, M. L. Temperature Dependence of the Rigid Amorphous Fraction in Poly(ethylene Terephthalate). *Eur. Polym. J.* **2014**, *58*, 60–68. https://doi.org/10.1016/j.eurpolymj.2014.06.005.

(25) Righetti, M. C. Amorphous Fractions of Poly(lactic Acid). In *Synthesis, Structure and Properties of Poly(lactic acid)*; Advances in Polymer Science; Springer, Cham, 2017; pp 195–234. https://doi.org/10.1007/12_2016_14.

(26) Parodi, E.; Govaert, L.; Peters, G. W. M. Glass Transition Temperature versus Structure of Polyamide 6: A Flash-DSC Study. *Thermochim. Acta* **2017**, *657*, 110–122. https://doi.org/10.1016/j.tca.2017.09.021.

(27) Di Lorenzo, M. L.; Righetti, M. C. Effect of Thermal History on the Evolution of Crystal and Amorphous Fractions of poly[(R)-3-Hydroxybutyrate] upon Storage at Ambient Temperature. *Eur. Polym. J.* **2013**, *49* (2), 510–517. https://doi.org/10.1016/j.eurpolymj.2012.11.004.

(28) Androsch, R.; Wunderlich, B. The Link between Rigid Amorphous Fraction and Crystal Perfection in Cold-Crystallized Poly(ethylene Terephthalate). *Polymer* **2005**, *46* (26), 12556–12566. https://doi.org/10.1016/j.polymer.2005.10.099.

(29) Kolesov, I.; Mileva, D.; Androsch, R. Mechanical Behavior and Optical Transparency of Polyamide 6 of Different Morphology Formed by Variation of the Pathway of Crystallization. *Polym. Bull.* **2014**, *71* (3), 581–593. https://doi.org/10.1007/s00289-013-1079-9.

(30) Di Lorenzo, M. L.; Righetti, M. C.; Wunderlich, B. Influence of Crystal Polymorphism on the Three-Phase Structure and on the Thermal Properties of Isotactic Poly(1-Butene). *Macromolecules* **2009**, *42* (23), 9312–9320. https://doi.org/10.1021/ma901882g.

(31) Esposito, A.; Delpouve, N.; Causin, V.; Dhotel, A.; Delbreilh, L.; Dargent, E. From a Three-Phase Model to a Continuous Description of Molecular Mobility in Semicrystalline Poly(hydroxybutyrate-Co-Hydroxyvalerate). *Macromolecules* **2016**, *49* (13), 4850–4861. https://doi.org/10.1021/acs.macromol.6b00384.

(32) Struik, L. C. E. Physical Aging in Plastics and Other Glassy Materials. *Polym. Eng. Sci.* **1977**, *17* (3), 165–173. https://doi.org/10.1002/pen.760170305.

(33) Hutchinson, J. M. Physical Aging of Polymers. *Prog. Polym. Sci.* **1995**, *20* (4), 703–760. https://doi.org/10.1016/0079-6700(94)00001-I.

(34) Boyd, R. H. Relaxation Processes in Crystalline Polymers: Molecular Interpretation — a Review. *Polymer* **1985**, *26* (8), 1123–1133. https://doi.org/10.1016/0032-3861(85)90240-X.

(35) Righetti, M. C.; Prevosto, D.; Tombari, E. Time and Temperature Evolution of the Rigid Amorphous Fraction and Differently Constrained Amorphous Fractions in PLLA. *Macromol. Chem. Phys.* **2016**, *217* (18), 2013–2026. https://doi.org/10.1002/macp.201600210.

(36) Righetti, M. C.; Mele, E. Structural Relaxation in PLLA: Contribution of Different Scale Motions. *Thermochim. Acta* **2019**, *672*, 157–161. https://doi.org/10.1016/j.tca.2018.12.027.

(37) Righetti, M. C.; Gazzano, M.; Delpouve, N.; Saiter, A. Contribution of the Rigid Amorphous Fraction to Physical Ageing of Semi-Crystalline PLLA. *Polymer* **2017**, *125*, 241–253. https://doi.org/10.1016/j.polymer.2017.07.089.

(38) Monnier, X.; Delpouve, N.; Saiter-Fourcin, A. Distinct Dynamics of Structural Relaxation in the Amorphous Phase of poly(L-Lactic Acid) Revealed by Quiescent Crystallization. *Soft Matter* **2020**, *16* (13), 3224–3233. https://doi.org/10.1039/C9SM02541C.

(39) Xu, H.; Ince, B. S.; Cebe, P. Development of the Crystallinity and Rigid Amorphous Fraction in Cold-Crystallized Isotactic Polystyrene. *J. Polym. Sci. Part B Polym. Phys.* **2003**, *41* (23), 3026–3036. https://doi.org/10.1002/polb.10625.

(40) Xu, H.; Cebe, P. Heat Capacity Study of Isotactic Polystyrene: Dual Reversible Crystal Melting and Relaxation of Rigid Amorphous Fraction. *Macromolecules* **2004**, *37* (8), 2797–2806. https://doi.org/10.1021/ma035961n.

(41) Righetti, M. C.; Di Lorenzo, M. L.; Tombari, E.; Angiuli, M. The Low-Temperature Endotherm in Poly(ethylene Terephthalate): Partial Melting and Rigid Amorphous Fraction Mobilization. *J. Phys. Chem. B* **2008**, *112* (14), 4233–4241. https://doi.org/10.1021/jp076399w.

(42) Di Lorenzo, M. L. The Melting Process and the Rigid Amorphous Fraction of Cis-1,4-Polybutadiene. *Polymer* **2009**, *50* (2), 578–584. https://doi.org/10.1016/j.polymer.2008.11.025.

(43) Di Lorenzo, M. L.; Gazzano, M.; Righetti, M. C. The Role of the Rigid Amorphous Fraction on Cold Crystallization of Poly(3-Hydroxybutyrate). *Macromolecules* **2012**, *45* (14), 5684–5691. https://doi.org/10.1021/ma3010907.

(44) Beckingham, B. S.; Ho, V.; Segalman, R. A. Formation of a Rigid Amorphous Fraction in Poly(3-(2'-Ethyl)hexylthiophene). *ACS Macro Lett.* **2014**, *3* (7), 684–688. https://doi.org/10.1021/mz500262d.

(45) Van den Brande, N.; Van Assche, G.; Van Mele, B. Thermal Behaviour below and inside the Glass Transition Region of a Submicron P3HT Layer Studied by Fast Scanning Chip Calorimetry. *Polymer* **2016**, *83*, 59–66. https://doi.org/10.1016/j.polymer.2015.12.018.

(46) Struik, L. C. E. The Mechanical and Physical Ageing of Semicrystalline Polymers: 1. *Polymer* **1987**, *28* (9), 1521–1533. https://doi.org/10.1016/0032-3861(87)90353-3.

(47) Struik, L. C. E. The Mechanical Behaviour and Physical Ageing of Semicrystalline Polymers: 2. *Polymer* **1987**, *28* (9), 1534–1542. https://doi.org/10.1016/0032-3861(87)90354-5.

(48) Pan, P.; Inoue, Y. Polymorphism and Isomorphism in Biodegradable Polyesters. *Prog. Polym. Sci.* **2009**, *34* (7), 605–640. https://doi.org/10.1016/j.progpolymsci.2009.01.003.

(49) Pan, P.; Zhu, B.; Kai, W.; Dong, T.; Inoue, Y. Effect of Crystallization Temperature on Crystal Modifications and Crystallization Kinetics of poly(L-Lactide). *J. Appl. Polym. Sci.* **2008**, *107* (1), 54–62. https://doi.org/10.1002/app.27102.

(50) Lotz, B. Crystal Polymorphism and Morphology of Polylactides. In *Synthesis, Structure and Properties of Poly(lactic acid)*; Advances in Polymer Science; Springer, Cham, 2017; pp 273–302. https://doi.org/10.1007/12_2016_15.

(51) Androsch, R.; Di Lorenzo, M. L.; Schick, C. Crystal Nucleation in Random L/D-Lactide Copolymers. *Eur. Polym. J.* **2016**, *75*, 474–485. https://doi.org/10.1016/j.eurpolymj.2016.01.020.

(52) Di Lorenzo, M. L.; Androsch, R. Influence of A'-/α-Crystal Polymorphism on Properties of Poly(l-Lactic Acid). *Polym. Int.* **2019**, *68* (3), 320–334. https://doi.org/10.1002/pi.5707.

(53) Androsch, R.; Schick, C.; Lorenzo, M. L. D. Kinetics of Nucleation and Growth of Crystals of Poly(<Emphasis Type="SmallCaps">l</Emphasis>-Lactic Acid). In *Synthesis, Structure and Properties of Poly(lactic acid)*; Advances in Polymer Science; Springer, Cham, 2017; pp 235–272. https://doi.org/10.1007/12_2016_13.

(54) Cangialosi, D.; Alegría, A.; Colmenero, J. Cooling Rate Dependent Glass Transition in Thin Polymer Films and in Bulk. In *Fast Scanning Calorimetry*; Springer, Cham, 2016; pp 403–431. https://doi.org/10.1007/978-3-319-31329-0_13.

(55) Boucher, V. M.; Cangialosi, D.; Alegría, A.; Colmenero, J. Enthalpy Recovery in Nanometer to Micrometer Thick Polystyrene Films. *Macromolecules* **2012**, *45* (12), 5296–5306. https://doi.org/10.1021/ma300622k.

(56) Sarge, S. M.; Hemminger, W.; Gmelin, E.; Höhne, G. W. H.; Cammenga, H. K.; Eysel, W. Metrologically Based Procedures for the Temperature, Heat and Heat Flow Rate Calibration of DSC. *J. Therm. Anal.* **1997**, *49* (2), 1125–1134. https://doi.org/10.1007/BF01996802.

(57) Wurm, A.; Merzlyakov, M.; Schick, C. Reversible Melting Probed by Temperature Modulated Dynamic Mechanical and Calorimetric Measurements. *Colloid Polym. Sci.* **1998**, *276* (4), 289–296. https://doi.org/10.1007/s003960050242.

(58) Androsch, R.; Moon, I.; Kreitmeier, S.; Wunderlich, B. Determination of Heat Capacity with a Sawtooth-Type, Power-Compensated Temperature-Modulated DSC. *Thermochim. Acta* **2000**, *357–358*, 267–278. https://doi.org/10.1016/S0040-6031(00)00397-X.

(59) Pyda, M.; Bopp, R. C.; Wunderlich, B. Heat Capacity of Poly(lactic Acid). *J. Chem. Thermodyn.* **2004**, *36* (9), 731–742. https://doi.org/10.1016/j.jct.2004.05.003.

(60) Righetti, M. C.; Gazzano, M.; Di Lorenzo, M. L.; Androsch, R. Enthalpy of Melting of A'- and α-Crystals of Poly(l-Lactic Acid). *Eur. Polym. J.* **2015**, *70*, 215–220. https://doi.org/10.1016/j.eurpolymj.2015.07.024.

(61) Minakov, A. A.; Wurm, A.; Schick, C. Superheating in Linear Polymers Studied by Ultrafast Nanocalorimetry. *Eur. Phys. J. E* **2007**, *23* (1), 43–53. https://doi.org/10.1140/epje/i2007-10173-8.

(62) Ma, Q.; Georgiev, G.; Cebe, P. Constraints in Semicrystalline Polymers: Using Quasi-Isothermal Analysis to Investigate the Mechanisms of Formation and Loss of the Rigid Amorphous Fraction. *Polymer* **2011**, *52* (20), 4562–4570. https://doi.org/10.1016/j.polymer.2011.08.006.

(63) Androsch, R.; Jariyavidyanont, K.; Schick, C. Enthalpy Relaxation of Polyamide 11 of Different Morphology Far Below the Glass Transition Temperature. *Entropy* **2019**, *21* (10), 984. https://doi.org/10.3390/e21100984.

(64) Berens, A. R.; Hodge, I. M. Effects of Annealing and Prior History on Enthalpy Relaxation in Glassy Polymers. 1. Experimental Study on Poly(vinyl Chloride). *Macromolecules* **1982**, *15* (3), 756–761. https://doi.org/10.1021/ma00231a015.

(65) Perez-de-Eulate, N. G.; Sferrazza, M.; Cangialosi, D.; Napolitano, S. Irreversible Adsorption Erases the Free Surface Effect on the Tg of Supported Films of Poly(4-Tert-Butylstyrene). *ACS Macro Lett.* **2017**, *6* (4), 354–358. https://doi.org/10.1021/acsmacrolett.7b00129.

(66) Boucher, V. M.; Cangialosi, D.; Alegría, A.; Colmenero, J. Reaching the Ideal Glass Transition by Aging Polymer Films. *Phys. Chem. Chem. Phys.* **2017**, *19* (2), 961–965. https://doi.org/10.1039/C6CP07139B.

(67) Monnier, X.; Saiter, A.; Dargent, E. Vitrification of PLA by Fast Scanning Calorimetry: Towards Unique Glass above Critical Cooling Rate? *Thermochim. Acta* **2017**, *658*, 47–54. https://doi.org/10.1016/j.tca.2017.10.019.

(68) Cangialosi, D. Dynamics and Thermodynamics of Polymer Glasses. *J. Phys. Condens. Matter* **2014**, *26* (15), 153101. https://doi.org/10.1088/0953-8984/26/15/153101.

(69) Yasuniwa, M.; Tsubakihara, S.; Iura, K.; Ono, Y.; Dan, Y.; Takahashi, K. Crystallization Behavior of Poly(l-Lactic Acid). *Polymer* **2006**, *47* (21), 7554–7563. https://doi.org/10.1016/j.polymer.2006.08.054.

(70) Zhuravlev, E.; Schmelzer, J. W. P.; Wunderlich, B.; Schick, C. Kinetics of Nucleation and Crystallization in Poly(ε-Caprolactone) (PCL). *Polymer* **2011**, *52* (9), 1983–1997. https://doi.org/10.1016/j.polymer.2011.03.013.

(71) Androsch, R.; Schick, C. Interplay between the Relaxation of the Glass of Random L/D-Lactide Copolymers and Homogeneous Crystal Nucleation: Evidence for Segregation of Chain Defects. *J. Phys. Chem. B* **2016**, *120* (19), 4522–4528. https://doi.org/10.1021/acs.jpcb.6b03022.